Lattice Boltzmann schemes for the nonlinear Schrödinger equation

Linhao Zhong* and Shide Feng
Laboratory of Cloud-Precipitation Physics and Severe Storms (LACS), Institute of Atmospheric Physics, Chinese Academy of Sciences, Beijing 100029, China

Ping Dong
Division of Civil Engineering, School of Engineering and Physical Sciences, University of Dundee, Dundee DD1 4HN, United Kingdom

Shouting Gao
Laboratory of Cloud-Precipitation Physics and Severe Storms (LACS), Institute of Atmospheric Physics, Chinese Academy of Sciences, Beijing 100029, China

(Received 22 January 2006; revised manuscript received 13 July 2006; published 25 September 2006)

The lattice Boltzmann (LB) method is applied to solve the time-dependent nonlinear Schrödinger (NLS) equation. Through approximating the reaction term at different orders of accuracy, three diffusion-reaction LB schemes are constructed for the cubic NLS equation. A LB initial condition is proposed to include the first-order nonequilibrium distribution function. These LB schemes are used to solve the one-soliton propagation and the homoclinic orbit problems. Detailed simulation results confirm that the high-order reaction term and the LB initial condition are effective in reducing the truncation errors. Compared with the Crank-Nicolson finite difference scheme, the LB scheme is found to give at least comparable and generally more accurate approximation for the cubic NLS equation.

DOI: 10.1103/PhysRevE.74.036704 PACS number(s): 02.70.−c, 02.60.Cb, 05.20.Dd

I. INTRODUCTION

As a numerical tool for studying fluid dynamics, lattice Boltzmann method (LBM) has been widely used in many research fields [1,2]. The desirable features of LBM, such as simple algorithm, convenience for boundary condition treatment and amenability to parallel computing, etc., are well documented [3,4].

The basic idea of LBM is to use a simple microscopic model of a fluid flow, usually involving a small number of discrete particle velocities, which is nevertheless capable of correctly describing the macroscopic flow behavior as the macroscopic partial differential equations (PDEs) recovered from the microscopic model conserving desired physical quantities and leading to correct fluxes of the conserved quantities [3]. For the Navier-Stokes equations, lattice Boltzmann (LB) models can be constructed by following some standard procedures that satisfy the mass and momentum conservation. However, as a numerical method for solving PDE, this "bottom-up" approach is often considered not as flexible as the conventional numerical methods, such as the finite difference method, whose starting point is the macroscopic PDE. Therefore, in order to encourage the wider use of LB models, it is necessary to demonstrate the superiority of LB model for different types of PDEs in numerical performance.

The slowly varying dispersive wave envelope is an important phenomenon existing in weakly nonlinear systems, where the nonlinear Schrödinger (NLS) equation plays a ubiquitous role. In plasma physics [5,6], nonlinear optics [7,8] and the atmospheric planetary-scale blocking flow [9,10], NLS equations of varying forms have been shown to capture the essential nonlinear systems behavior. One of the most widely used NLS equations is the cubic NLS equation, which may be written as [11]

$$i\frac{\partial u}{\partial t}+\frac{\partial^2 u}{\partial x^2}+2V(|u|)u=0, \tag{1}$$

where i is the imaginary unit and $V(|u|)=|u|^2$ is the external potential. Analytical and numerical investigations have been carried out on this equation by many authors [11–14].

Associated with the nonrelativistic Schrödinger equation and the relativistic Dirac equation, the quantum lattice-gas algorithms have been studied since the mid-1990s. Bialynicki-Birula [15] introduced a unitary cellular-automata model on a three-dimensional cubic lattice to simulate the Weyl, Dirac, and Maxwell equations. Along this line, Meyer [16,17] presented a one-dimensional quantum algorithm to efficiently simulate different physical processes. Boghosian and Taylor [18–20] considered a general class of the classic lattice gas models. They have shown that a kinetic transport equation at the "microscopic scale" leads to the Schrödinger equation at the continuum limit in an arbitrary number of dimensions and can be extended to describe nonrelativistic many-body physics. Contemporaneously with the above works, Succi and Benzi [21], and Succi [22] found that the Dirac equation leads to the nonrelativistic Schrödinger equation in the long wavelength hydrodynamic limit in much the same way as the lattice Boltzmann equation (LBE) leads to the Navier-Stokes equations. By using the operator splitting method, they presented a lattice gas model in which the Dirac equation in the Majorana representation evolves as a

*Electronic address: zlh@mail.iap.ac.cn

sequence of three one-dimensional LBEs with complex-valued distribution functions. This quantum lattice gas algorithm has been validated for both the linear Schrödinger equation [22] and the nonlinear Schrödinger equation relating to Bose-Einstein condensation [23]. Yepez [24] presented a factorized quantum lattice gas model to simulates mesoscopic dynamics of an ensemble of classical lattice gases. The quantum lattice-gas models replace the digital bits used in classical lattice-gas models with the quantum bits and has the system wave function collapsed into a tensor product state over the quantum bits after each collision step. This feature results in the local entanglement over nearby quantum bits for only a short time period, which makes the algorithms suitable for implementation on the type II quantum computers, an array of small quantum computers interconnected by classical communication network [25]. This quantum lattice gas model is a noiseless, unconditionally stable method and has been applied to the fluid flows [24], the diffusion equation [26] and the Burgers equation [27]. Yepez and Boghosian [28,29] presented a quantum lattice-gas model for the many-body Schrödinger wave equation and reproduced the correct dynamical behavior of the wave function in the presence of an external potential. By use of the same quantum lattice gas model, Vahala *et al.* [30] were able to produce the correct soliton solutions of the cubic NLS equation.

Motivated by the above works, we intend to establish in this paper a direct connection between the mesoscopic LBE and the macroscopic NLS equation. Differing from the quantum LBEs used in Refs. [21–23], where the linear or nonlinear Schrödinger equations are simulated by the Dirac equation, the starting point of our models is the LBE with the complex-valued distribution function and relaxation time. In the lattice gas model presented in Refs. [20,29], a local phase change to the system wave function is used as

$$u(x,t) \to e^{[2iV(x)\Delta t]}u(x,t), \tag{2}$$

which converges to the NLS equation in the continuum limit, $\Delta t \to 0$. Because of the close theoretical connections between lattice-gas method and LBM, this phase change suggests that NLS equation may also be derived from LBE with some necessary modifications.

Based on the above observations, the work reported here is carried out. The paper is organized as follow. In the next section, a set of modified LB schemes with different orders of accuracy is constructed to solve the cubic NLS equation. In Sec. III, a nonequilibrium initial condition for the LBE is presented for the purpose of reducing the error arising from the equilibrium-distribution initialization algorithm. In order to test these numerical schemes and the initialization algorithm, in Sec. IV we will mainly examine two problems, the one-soliton solution and the homoclinic orbits problem. The numerical results are evaluated by comparing them with both exact solutions and the numerical solutions obtained by using a classic finite difference scheme, the Crank-Nicolson (CN) scheme. In the last section, we discuss the implications of the results and conclude the paper.

II. LATTICE BOLTZMANN SCHEMES FOR NLS EQUATION

A. General description

Without external potential term, the NLS equation, Eq. (1), has the same form as the standard diffusion equation except that the "mass density" and "diffusion coefficient" are all complex valued. Chen *et al.* [31] showed that the diffusion equation can be derived from the LBE at $O(\varepsilon^2)$, where ε is the Knudsen number given by the ratio of characteristic length of fluid and the mean free path of the particle. For Eq. (1), the external potential may be introduced by making use of the transformation Eq. (2) in the LBE as

$$f_j(x+\Delta x_j, t+\Delta t) = e^{[2iV(x,t)\Delta t]}f_j(x,t) - \frac{1}{\tau}[f_j(x,t) - f_j^{(\mathrm{eq})}(x,t)], \tag{3}$$

where $f_j(x,t)$ is the particle distribution function at (x,t) in the direction of the one-dimensional particle velocity c_j; $j=0,1,2,\ldots,N$ is the index for the discrete velocity set $\{c_0,c_1,c_2,\ldots,c_N\}$; $f_j^{(\mathrm{eq})}(x,t)$ is the local equilibrium distribution function; Δt and Δx_j are, respectively, the discrete time interval and discrete space interval in j direction with the constraint $\Delta x_j = c_j \Delta t$, which results to the standard collision-streaming algorithm. By the use of the diffusive scaling [32,33], the assumptions $|\Delta x_j| \sim O(\varepsilon)$ and $\Delta t \sim O(\varepsilon^2)$ are applied to Eq. (3). Through a regular expansion $f_j = f_j^{(0)} + \varepsilon f_j^{(1)} + \varepsilon^2 f_j^{(2)} + \cdots$, we obtain the Taylor expansion equations at different orders of ε,

$$O(1): f_j^{(0)} - f_j^{(\mathrm{eq})} = 0, \tag{4}$$

$$O(\varepsilon): c_j \frac{\partial f_j^{(0)}}{\partial x} + \frac{f_j^{(1)}}{\tau \Delta t} = 0, \tag{5}$$

$$O(\varepsilon^2): \frac{\partial f_j^{(0)}}{\partial t} - \Delta t\left(\tau - \frac{1}{2}\right)c_j^2 \frac{\partial^2 f_j^{(0)}}{\partial x^2} - 2iVf_j^{(0)} + \frac{f_j^{(2)}}{\tau \Delta t} = 0. \tag{6}$$

Summing Eqs. (4)–(6) over index j and defining the moment constraints to only conserve the first moment,

$$u = \sum_{j=0}^{N} f_j = \sum_{j=0}^{N} f_j^{(\mathrm{eq})}, \tag{7}$$

$$0 = \sum_{j=0}^{N} c_j f_j^{(\mathrm{eq})}, \tag{8}$$

the macroscopic NLS equation can be derived at $O(\varepsilon^2)$,

$$\frac{\partial u}{\partial t} - \Delta t\left(\tau - \frac{1}{2}\right)c_s^2 \frac{\partial^2 u}{\partial x^2} - 2iV(|u|)u = 0, \tag{9}$$

where c_s is the lattice sound speed [34], which is defined by the second-order moment,

$$uc_s^2 = \sum_{j=0}^{N} c_j^2 f_j^{(\mathrm{eq})}. \tag{10}$$

In the limit $\varepsilon \to 0$, the cubic NLS equation (1) is recovered from Eq. (9) by defining the complex relaxation time as $\tau = (2i + c_s^2 \Delta t)/(2c_s^2 \Delta t)$.

B. LB schemes with different reaction term

In fact, Eq. (3) has the same form as the standard LBE for diffusion-reaction problem [31]. By expanding the external potential term of Eq. (3) up to $O(\Delta t^2)$,

$$e^{[2iV(x,t)\Delta t]} = 1 + 2iV(x,t)\Delta t + O(\Delta t^2),$$

the LBE has the form

$$f_j(x + \Delta x_j, t + \Delta t) = f_j(x,t) - \frac{1}{\tau}[f_j(x,t) - f_j^{(\mathrm{eq})}(x,t)] + 2iV(x,t) f_j(x,t)\Delta t, \tag{11}$$

where the high-order term of $O(\Delta t^2)$ has been omitted. On the right-hand side of Eq. (11), the last term which is the order of $O(\varepsilon^2)$ is analogous to the reaction term in the diffusion-reaction LB scheme [31] except that it is complex valued. Hence as the standard LB scheme, the dynamics of Eq. (11) can also be split into the two separate processes, namely collision and streaming.

To improve the accuracy of the LB scheme (11), two modified schemes with higher-order discretization of reaction term are presented below. First, the second-order time integral along a characteristic [35] maybe applied to the reaction term

$$f_j(x + \Delta x_j, t + \Delta t) = f_j(x,t) - \frac{1}{\tau}[f_j(x,t) - f_j^{(\mathrm{eq})}(x,t)] + i\Delta t[V(x,t) f_j(x,t) + V(x + \Delta x_j, t + \Delta t) \times f_j(x + \Delta x_j, t + \Delta t)]. \tag{12}$$

In the practical simulation, it is found that only three to four prediction-correction iterations in streaming step would be sufficient for stable numerical integration although the reaction term has implicit feature in Eq. (12). Applying the diffusive scaling to Eqs. (11) and (12) in a similar way as that presented in the preceding section, the macroscopic equations of the same form as Eq. (9) at $O(\varepsilon^2)$ can be obtained. That is to say, both schemes [Eqs. (11) and (12)] approximate NLS equation up to $O(\varepsilon^2)$.

We may further transform Eq. (12) into

$$f_j(x + \Delta x_j, t + \Delta t) = f_j(x,t) - \frac{1}{\tau}[f_j(x,t) - f_j^{(\mathrm{eq})}(x,t)] + i\Delta t[V(x,t) R_j(x,t) + V(x + \Delta x_j, t + \Delta t) R_j(x + \Delta x_j, t + \Delta t)], \tag{13}$$

where the distribution function in the reaction term has been replaced with an undetermined variable $R_j(x,t)$. To obtain the form of $R_j(x,t)$, we first expand Eq. (13) up to $O(\varepsilon^4)$ according to the diffusive scaling [32,33]. The resulting macroscopic equations at the first three orders of ε have the same forms as those obtained from Eqs. (4)–(6) with the moment relations being defined as

$$u = \sum_{j=0}^{N} R_j, \tag{14}$$

$$0 = \sum_{j=0}^{N} c_j R_j. \tag{15}$$

Note that the number of the undetermined variable R_j is the same as the total number of the discrete particle velocity. In the next section, a rest particle accounting for a given ratio to total equilibrium particles, viz. $f_0^{(\mathrm{eq})}/\Sigma_{j=0}^{N} f_j^{(\mathrm{eq})} = d_0$, is imposed to the simplest models of schemes (11)–(13). With this additional constraint, the form of the equilibrium distribution function can be obtained by the constraints Eqs. (7) and (8). Here we also assume that the function R_j has the similar form as the equilibrium distribution but without the constraint $R_0/\Sigma_{j=0}^{N} R_j = d_0$. Apart from the two constraints, Eqs. (14) and (15), a third constraint would be needed. One of the reasonable choices is the second-order particle-velocity moment of R_j. However, only the zeroth-order moment and the first-order moment are obtained from the equations up to $O(\varepsilon^2)$. This makes the system still undetermined for R_j. To obtain the second-order moment of R_j, we may resort to the equation at higher-order equations, such as equations at $O(\varepsilon^3)$ and $O(\varepsilon^4)$. But the equation at the third order of ε has no contribution to the final macroscopic equation because of the constraints Eqs. (8) and (15). Hence, the additional constraint for R_j must be found through the macroscopic equation at $O(\varepsilon^4)$,

$$\frac{i\Delta t^2}{2}\left((2\tau - 1)^2 \frac{\partial^2 [V(x,t)\Gamma_2(x,t)]}{\partial x^2} - c_s^2 (8\tau^2 - 8\tau + 1) \times \frac{\partial^2 [V(x,t) u(x,t)]}{\partial x^2} \right) + O(\Delta t^3) = 0, \tag{16}$$

where $\Gamma_2(x,t) = \Sigma_{j=0}^{N} c_j^2 R_j(x,t)$ is the second-order moment of R_j. Obviously, the terms of $O(\Delta t^2)$ in Eq. (16) are errors resulted from the external potential. Equation (16) provides a means to define the second-order moment of R_j with twofold uses that can determine R_j and eliminate part of the errors resulted from external potential at the same time. In fact, the errors of $O(\Delta t^2)$ in Eq. (16) exist in the scheme (11) and (12), but they are canceled by defining the second-order moment constraint,

$$\Gamma_2(x,t) = \frac{c_s^2 (8\tau^2 - 8\tau + 1)}{(2\tau - 1)^2} u(x,t). \tag{17}$$

Now Eqs. (14), (15), and (17) are a closed system for determining R_j in a given particle model.

C. Implements of the LB schemes

To solve the diffusion-reaction problem, $\pi/2$ rotational invariance is sufficient to yield full isotropy [36]. For the

one-dimensional diffusion-reaction equation similar to the cubic NLS Eq. (1), one of the simplest LB models is the 3-bit model, which includes one rest particle and two moving particles with the same speed in opposite directions at each spatial node, viz. $(c_0,c_1,c_2)=(0,c,-c)$. For such a LB model, the equilibrium distribution $f_j^{(\mathrm{eq})}$ and the lattice sound speed satisfying Eqs. (7), (8), and (10) are

$$f_j^{(\mathrm{eq})}=\begin{cases} d_0 u, & j=0, \\ \dfrac{(1-d_0)}{2}u, & j=1,2, \end{cases} \tag{18}$$

$$c_s=\sqrt{(1-d_0)}c, \tag{19}$$

where the real number $d_0=f_0^{(\mathrm{eq})}/\Sigma_{j=0}^{N}f_j^{(\mathrm{eq})}$ represents the fraction of the rest particle at each node. In a similar way, the term R_j in Eq. (13) is calculated from the moment relations Eqs. (14), (15), and (17),

$$R_j=\begin{cases} \dfrac{d_0(8\tau^2-8\tau+1)-4\tau(\tau-1)}{(2\tau-1)^2}u, & j=0, \\ \dfrac{(1-d_0)(8\tau^2-8\tau+1)}{2(2\tau-1)^2}u, & j=1,2. \end{cases} \tag{20}$$

For the schemes (11) and (12), because the reaction term is expressed in terms of the distribution function, the fraction of the reaction term in the direction c_0 is approximately d_0, which equals to the fraction of the rest particle in equilibrium distribution (18). As a result, d_0 is a free parameter that can be set to any value in the range $0\leqslant d_0<1$. However the lower limit does not apply to scheme (13), where the reaction term is determined by the constraints Eqs. (14), (15), and (17). As shown by Eq. (20), we have $R_0/(R_1+R_2)\neq d_0$ which means that some proportion of the reaction term must be taken on by the rest particle, i.e., the model requires $d_0\neq 0$. Without loss of generality, d_0 is fixed at 1/3 for all the three LB schemes presented above in the simulations.

III. NUMERICAL EXPERIMENT DESIGN

A. Model problems

For the purpose of evaluating the numerical schemes for the cubic NLS equation Eq. (1), the soliton solution is an excellent test case. Therefore, the first problem considered in this paper is the one-soliton propagation problem with the initial value

$$u(x,0)=\mathrm{sech}(x+15)e^{i(3/2)(x+15)}. \tag{21}$$

The analytical solution for this problem is

$$u(x,t)=\mathrm{sech}(x+15-3t)e^{i(1/4)(6x-5t+90)}, \tag{22}$$

which describes a soliton-type wave envelope traveling along the x axis from left to right with a group velocity of 3, amplitude of 1, and the initial peak value at $x=-15$. Our simulations are confined to $0\leqslant t\leqslant 10$ and $-40\leqslant x\leqslant 40$ with periodic boundary conditions.

Ablowitz and Clarkson [37] expounded the homoclinic structure and numerically induced chaos for the cubic NLS equation. They found that the numerical homoclinic instability is manifested in many numerical schemes employed to solve the cubic NLS equation. The homoclinic instability triggered by numerical rounding error will disappear only when the grid is sufficiently refined [37]. It is therefore reasonable to expect that if a numerical scheme is good it should be able to avoid destabilizing the homoclinic orbits of NLS equation even when relatively coarse spatial resolution is used. We consider this sensitivity problem caused by the homoclinic structure as an important test for the numerical schemes for NLS equation. As the second numerical test, we implemented the LB schemes with the initial condition similar to those given in Ref. [11],

$$u(x,0)=0.5-0.05\cos\left(\frac{2\pi}{L}x\right) \tag{23}$$

by defining the spatial range, $0\leqslant x\leqslant L$ and $L=2\sqrt{2}m\pi$ with $m=1,2$. Under this initial condition, the solution of the NLS equation has only one unstable mode and a single homoclinic orbit for $m=1$, and two single homoclinic orbits and a combination orbit for $m=2$ [11]. For this problem, each scheme considered will be integrated over the time range of $0\leqslant t\leqslant 300$.

B. Initialization for LB schemes

Besides the macroscopic initial condition Eqs. (21) and (23), the initial condition at microscopic level must also be given for the distribution in LBM. Inconsistent initial conditions that lead to initial layers may reduce the theoretically possible accuracy of the schemes [38]. Generally, the initialization considers that the particles satisfy equilibrium distribution

$$f_j(x,0)=f_j^{(\mathrm{eq})}[u(x,0)]. \tag{24}$$

This is a first-order approximation of distribution f_j as it retains only the first term in the expansion $f_j=f_j^{(\mathrm{eq})}+\varepsilon f_j^{(1)}+\varepsilon^2 f_j^{(2)}+\cdots$. Consequently, the high-order term $f_j^{(n)}$ $(n\geqslant 1)$ has no contribution to the initial value of the macroscopic "mass" as shown by Eq. (7). Although the initial condition Eq. (24) does not affect the macroscopic equations at the first two orders of ε, it leads to the wrong dissipation coefficient in the equation at $O(\varepsilon^2)$ in the initialization process. This inconsistency originates from disappearance of the collision term in the initialization routine (24). In Eq. (9), part of diffusion term, $\Delta t\tau c_s^2(\partial^2 u/\partial x^2)$, comes from the nonequilibrium correction to the equilibrium distribution in the collision term of Eq. (3), viz. $(f_j-f_j^{(\mathrm{eq})})$. It is manifest that part of the diffusion term will disappear with the collision term when the particles are in the equilibrium states. However, in the overall numerical integration, the diffusion coefficient is set to be $\Delta t(\tau-1/2)c_s^2$, which implies that the use of the initial condition (24) causes inconsistencies in the initialization due to the diffusion error.

Some recent works [38,39] have studied nonequilibrium initial conditions for the LBM applied to the Navier-Stokes equations. In these initialization processes, the fluid density was considered as the only conserved variable and the fluid velocity was fixed at the initial value. The initialization may be thought of as a linear time-dependent diffusion-advection equation for a passive scalar (fluid density) with a given advective velocity (fluid velocity) and a mass forcing term determined by the imposed fluid momentum relevant to the given initial velocity. A LBE for the diffusion-advection equation was integrated until the distribution function reached steady state. Through this initialization procedure subject to the given fluid velocity, they obtained the distribution function comprising nonequilibrium part, which was considered as the initial value of the LB scheme for the Navier-Stokes equations. But for the problem considered in this paper, a complex-valued passive scalar (u) is the only conserved variable. The iterative procedures similar to those in Refs. [38,39] were found to be ineffective because the NLS equation itself has the form of diffusion equation.

It is noticed that the lost diffusion $[\Delta t \tau c_s^2(\partial^2 u/\partial x^2)]$ in the initialization (24) stems from the first-order nonequilibrium part of distribution function ($f_j^{(1)}$) in the diffusive scaling procedure (4)–(9). This diffusion error may be eliminated by including the high-order correction ($f_j^{(1)}$). By using Eqs. (4) and (5), the first-order nonequilibrium part expressed by $f_j^{(\mathrm{eq})}$ is added to the initial condition as

$$f_j(x,0) = f_j^{(\mathrm{eq})}[u(x,0)] - \tau \Delta t c_j \frac{\partial f_j^{(\mathrm{eq})}[u(x,0)]}{\partial x}. \tag{25}$$

Obviously, the nonequilibrium part in Eq. (25) has no influence on implementing the initialization subject for a given $u(x,0)$ because of the moment constraint Eq. (8). The spatial derivative of $f_j^{(\mathrm{eq})}$ in Eq. (25) can be expressed exactly for a given $u(x,0)$ with a functional expression or be approximated numerically when such a functional expression is not available. By substituting Eqs. (21) and (23) into Eq. (25), the initial conditions of LBE for the problems discussed in this work are formulated in a general form as

$$f_j(x,0) = \begin{cases} d_0 F_j(x), & j = 0, \\ \dfrac{(1-d_0)}{2} F_j(x), & j = 1,2, \end{cases} \tag{26}$$

where the function $F_j(x)$ reads

$$F_j(x) = \tau \Delta t \left[c_j \tanh(x+15) + \left(\frac{1}{\tau \Delta t} - \frac{3}{2} c_j i \right) \right] \times \mathrm{sech}(x+15) e^{[(3/2)i(x+15)]} \tag{27}$$

for the initial condition (21) and

$$F_j(x) = 0.5 - 0.05 \cos\left(\frac{2\pi x}{L}\right) - 0.1 \frac{\pi \tau \Delta t c_j}{L} \sin\left(\frac{2\pi x}{L}\right) \tag{28}$$

for the initial condition (23), respectively.

C. Evaluation method

For the two initial-boundary value problems described in Sec. III A, the cubic NLS equation should conserve following two variables [11,12]:

$$H(t) = \int |u(x,t)|^2 dx, \tag{29}$$

$$E(t) = \int [|u_x(x,t)|^2 - |u(x,t)|^4] dx. \tag{30}$$

The integrals in Eqs. (29) and (30) are approximated discretely by the left Riemann sums when we calculate the values of H and E in numerical experiments. In a way similarly to the work in Ref. [14], three variables are used to evaluate the numerical results of each scheme,

$$S_1(t) = \left| \frac{H(t) - H(0)}{H(0)} \right|, \tag{31}$$

$$S_2(t) = \left| \frac{E(t) - E(0)}{E(0)} \right|, \tag{32}$$

$$P(t) = \frac{\max_x |u_n(x,t) - u(x,t)|}{\max_x |u(x,t)|}, \tag{33}$$

where $u_n(x,t)$ is the numerical solution at (x,t). The variable $S_1(t)$ and $S_2(t)$, respectively, describes the conservation accuracy of $H(t)$ and $E(t)$, and $P(t)$ represents the normalized error.

In order to validate the LB schemes presented here, we have performed all simulations based on a finite difference scheme and the LB schemes with the same parameter sets. An energy conserving Crank-Nicolson (CN) scheme [12] is chosen as a comparison scheme because of its popularity and robustness for solving the cubic NLS equation [11]. According to Ref. [12], the CN scheme for Eq. (1) has the form

$$\begin{aligned} &\frac{i}{\Delta t}[u(x,t) - u(x,t-\Delta t)] \\ &\quad + \frac{1}{2}\left(\frac{u(x+\Delta x,t) - 2u(x,t) + u(x-\Delta x,t)}{\Delta x^2} \right) \\ &\quad + \frac{1}{2}\left(\frac{u(x+\Delta x,t-\Delta t) - 2u(x,t-\Delta t) + u(x-\Delta x,t-\Delta t)}{\Delta x^2} \right) \\ &\quad + \frac{1}{2}[|u(x,t)|^2 + |u(x,t-\Delta t)|^2][u(x,t) + u(x,t-\Delta t)] = 0, \end{aligned} \tag{34}$$

where the constraint, $\Delta x = c\Delta t$, is imposed to obtain the same spatial resolution as the LB schemes in our numerical experiments. Through linearized stability analysis, scheme (34) is accurate to $O(\Delta x^2 + \Delta t^2)$ and unconditionally stable.

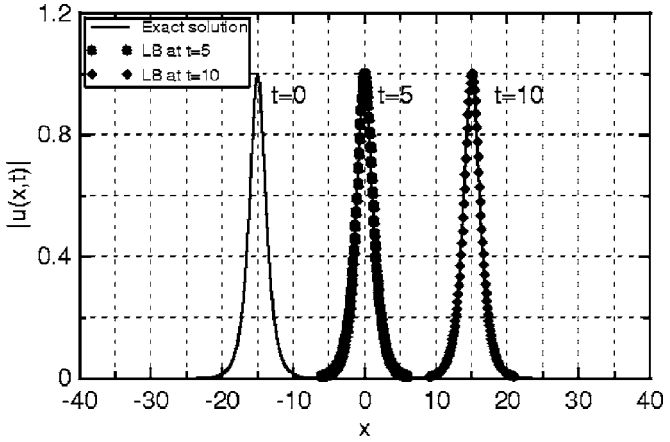

FIG. 1. One-soliton solution of the cubic NLS equation. The abscissa is the spatial variable x and the ordinate is the modulus of $u(x,t)$; lines and discrete symbols are the exact solutions (22) at $t=0,5,10$ and numerical solutions of LB-I with IC-I at $t=5,10$.

IV. NUMERICAL RESULTS

For the convenience of future referencing, we shall label the three LB schemes (11), (12), and (13) as LB-I, LB-II, and LB-III, respectively. Similarly, the initial conditions Eqs. (24) and (25) will be referred to as IC-I and IC-II, respectively.

A. Soliton solution

We first test the one-soliton propagation problem Eqs. (21) and (22) with fixed space interval $\Delta x=0.05$ but different time interval Δt which varies from 1×10^{-5} to 5×10^{-3}. Both the LB schemes and the CN scheme attain the best accuracy around $\Delta t=1\times10^{-4}$, which is equivalent to assume the Knudsen number $\varepsilon\sim(10^{-2})$. Figure 1 presents the comparison between the numerical solution of scheme LB-I with IC-I and the exact solution Eq. (22) for $\Delta t=1\times10^{-4}$ and $\Delta x=0.05$. It can be seen from this figure that the shape of the soliton is precisely preserved and the group velocity is also well simulated by scheme LB-I.

Table I lists the normalized error P and the conservation errors S_1 and S_2 of the four schemes at one time unit for this case. As shown by Table I, all three LB schemes attain the accuracy that is comparable to that of scheme CN. For the initial condition IC-I, the normalized error P of each LB scheme is slightly greater than that of scheme CN. It is noted that the accuracy is improved when the high-order reaction terms in Eqs. (12) and (13) are used. In particular, among the three LB schemes, scheme LB-III shows the best accuracy, which is very close to that of scheme CN. When the initial condition changes to IC-II, obvious improvement is found in the results of all three LB schemes. The normalized error of each LB scheme becomes less than the scheme CN, and the most obvious accuracy improvement is again found in scheme LB-III, whose error is only about 3% of that of scheme CN. Similar improvements can also be seen in the conservation error term S_2. For the conservation variable $E(t)$, the initial condition IC-II achieves most obvious improvement in scheme LB-III implying that it has better conservative property than scheme CN. But for S_1, although the corrected initial condition improves conservative accuracy, the error of LB scheme is still greater than that of scheme CN, whose error reaches the level of numerical round-off error from double-precision arithmetic as the CN scheme chosen here is designed to conserve exactly the discrete approximation to the quantity H.

TABLE I. Errors of different schemes at $t=1$ with $\Delta t=1\times10^{-4}$, $\Delta x=0.05$.

Numerical scheme		P (1)	S_1 (1)	S_2 (1)
LB-I	IC-I	8.543×10^{-3}	1.320×10^{-3}	1.642×10^{-3}
	IC-II	4.095×10^{-3}	8.648×10^{-4}	1.089×10^{-3}
LB-II	IC-I	7.072×10^{-3}	1.859×10^{-3}	2.255×10^{-3}
	IC-II	2.684×10^{-3}	3.252×10^{-4}	4.762×10^{-4}
LB-III	IC-I	4.575×10^{-3}	2.181×10^{-3}	2.729×10^{-3}
	IC-II	1.375×10^{-4}	9.689×10^{-7}	1.198×10^{-6}
C-N		4.097×10^{-3}	3.331×10^{-16}	1.210×10^{-5}

These results strongly indicate that the LB schemes attain the similar level of accuracy as the CN scheme and the corrected initial condition IC-II is able to reduce the truncation errors considerably. To further confirm this, several runs are performed to test the spatial accuracy order. In this set of runs, we take Δt proportional to Δx^2 with Δx varying from 0.04 to 0.1. The maximum error changes with Δx for each scheme are presented in Fig. 2. It shows clearly that schemes LB-I, LB-II, and LB-III with IC-I all attain the second-order spatial accuracy (as indicated by the slopes labeled in the figures). Moreover, because the reaction term in scheme LB-III cancels part of high-order errors resulted from external potential [shown by Eq. (16)], scheme LB-III has the best accuracy compared to the other two LB schemes with the same initialization routine. The other noticeable feature of Fig. 2 is that the initial condition IC-II is effective in reducing errors and dramatically improving accuracy. The initialization IC-II improves the spatial accuracies of schemes LB-II and LB-III from $O(\Delta x^2)$ to $O(\Delta x^4)$, which was also achieved by the quantum lattice gas presented in Ref. [29]. As pointed out in Sec. III B, the reaction terms of schemes LB-II and LB-III are designed to be theoretically accurate to $O(\Delta x^4)$, but the error caused by the initial layer due to the equilibrium initialization renders IC-I to be inaccurate with time integration. After this error was eliminated by replacing IC-I with IC-II, the schemes LB-II and LB-III attain the expected accuracies.

B. Simulations for homoclinic orbits

In the simulations of the second test problem (23), each numerical scheme is performed under several different spatial resolutions. Through changing the number of spatial grid points (N_g) used in simulation, we intend to determine the critical spatial resolution that is required to maintain correct homoclinic orbit. Additionally, in order to minimize the in-

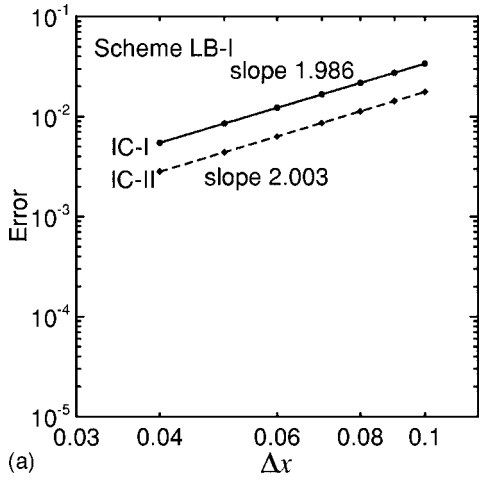

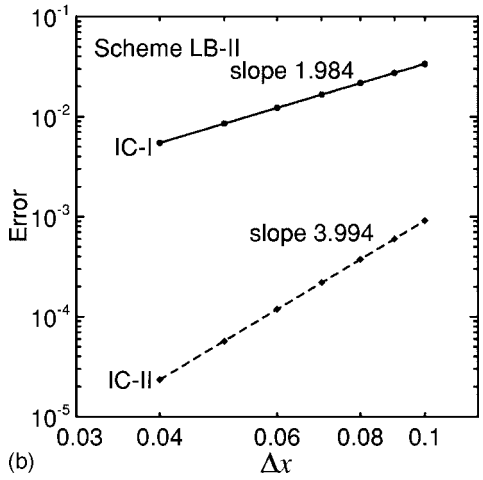

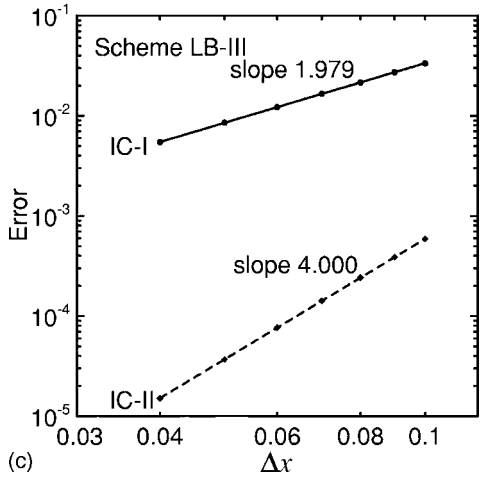

FIG. 2. Measurement of error convergence about the spatial interval Δx for LB schemes with different initial conditions. (a), (b), and (c) correspond to the results of schemes LB-I, LB-II, and LB-III, respectively. Discrete symbols represent the maximum value of the error across the whole spatial range at $t=\Delta t$ for each run. The experiments are performed from $\Delta x=0.04$ to 0.1 with $\Delta t=\Delta x^2$. The lines represent the linear fittings of the errors versus Δx in the logarithmic coordinate. The slopes of lines are labeled next to the corresponding lines.

fluence of the time discretization we have performed several runs with different values of Δt to achieve the best result for each spatial resolution (N_g).

When $m=1$ for Eq. (23), we perform the experiments with $N_g=30,28,24,16,12,10$, respectively. The critical resolution values are determined as 28, 12, 12, and 24 for schemes CN, LB-I, LB-II, and LB-III, respectively, and they appeared to be insensitive to the choice of the LB initial condition. All the LB schemes discussed here, especially LB-I and LB-II, are found to preserve the single homoclinic orbit better than scheme CN. Figure 3 illustrates the solutions obtained from scheme CN and scheme LB-I with IC-I for $N_g=12$. Even under such a coarse spatial resolution, scheme LB-I still preserves regular periodic oscillation. In comparison, the solution from scheme CN becomes chaotic over almost the entire integration time due to the numerical homoclinic instability.

When the value of m is increased to 2, we choose the number of the grid points ranging from 20 to 200 in simulations. Over the entire 300 time units, no schemes except LB-III were able to simulate well the three-homoclinic-orbit structure. As shown in Figs. 4(b) and 4(d) for $N_g=100$, the solution from LB-III is well behaved over the integration interval. But when the same parameter set is used for CN, the modulus of the solution oscillates irregularly as shown in Figs. 4(a) and 4(c). Although the LB-III results are not as good as that using the integrable scheme presented in Ref. [11], the LB-III still performs much better than the "standard" finite difference scheme discussed here.

V. CONCLUSION

In this paper, three LB schemes are applied to solve the cubic NLS equation. An initial condition for LBE with first-order nonequilibrium correction is proposed to eliminate the diffusion error in the initialization process. To evaluate the numerical schemes, numerical experiments are performed using both the LB schemes and the CN scheme for the problems of the one-soliton propagation and the numerical homoclinic instability.

Detailed studies of soliton solution problem have shown that the LB schemes have accuracy that is better than or at least comparable to the classic finite difference scheme considered in this paper. The high-order reaction term of LBE, especially that can cancel some high-order term introduced by external potential, improved the accuracy of the LB scheme significantly. It was also found that the initial condition performed well in reducing the truncation error for all the three LB schemes. In particular, the initial condition improved the accuracies of schemes LB-II and LB-III to $O(\Delta x^4)$. We also observed that none of the three LB schemes conserve the variable H as well as scheme CN although they achieved comparable or better conservation accuracy of variable E. This suggests that further improvements are still needed in the construction of the LB schemes.

For the numerical homoclinic instability problem, the number of the critical grid points used by the LB schemes to preserve the correct homoclinic orbit were found to be less than that used by scheme CN when the initial condition had single unstable mode. But for the case with two unstable

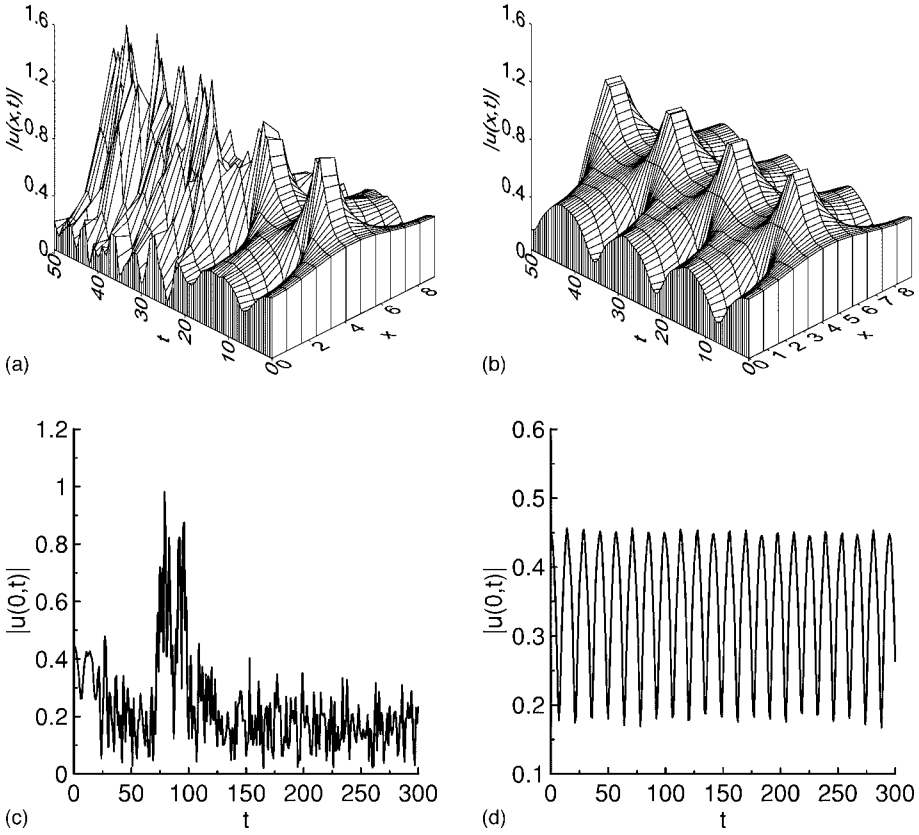

FIG. 3. Numerical simulations for the single-homoclinic-orbit ($m=1$) problem: (a) and (b) are time-space evolution of the modulus of $u(x,t)$ over the first 50 time units; (c) and (d) are the time evolution of the modulus of $u(0,t)$ over the whole integration interval. The spatial resolution is $N_g=12$. Results in (a) and (c) are calculated from scheme CN, and those in (b) an (d) from schemes LB-I with IC-I.

modes, almost all the LB schemes and scheme CN were shown to be unable to simulate the three-homoclinic-orbit structure. Only scheme LB-III was able to model the correct solution at $N_g=100$, which is a finer spatial resolution than that used in the integrable scheme presented by Ablowitz and Clarkson [11]. In the future work, some treatments about integrable property may be applied to the LB scheme in a way similar to that done to the conventional scheme.

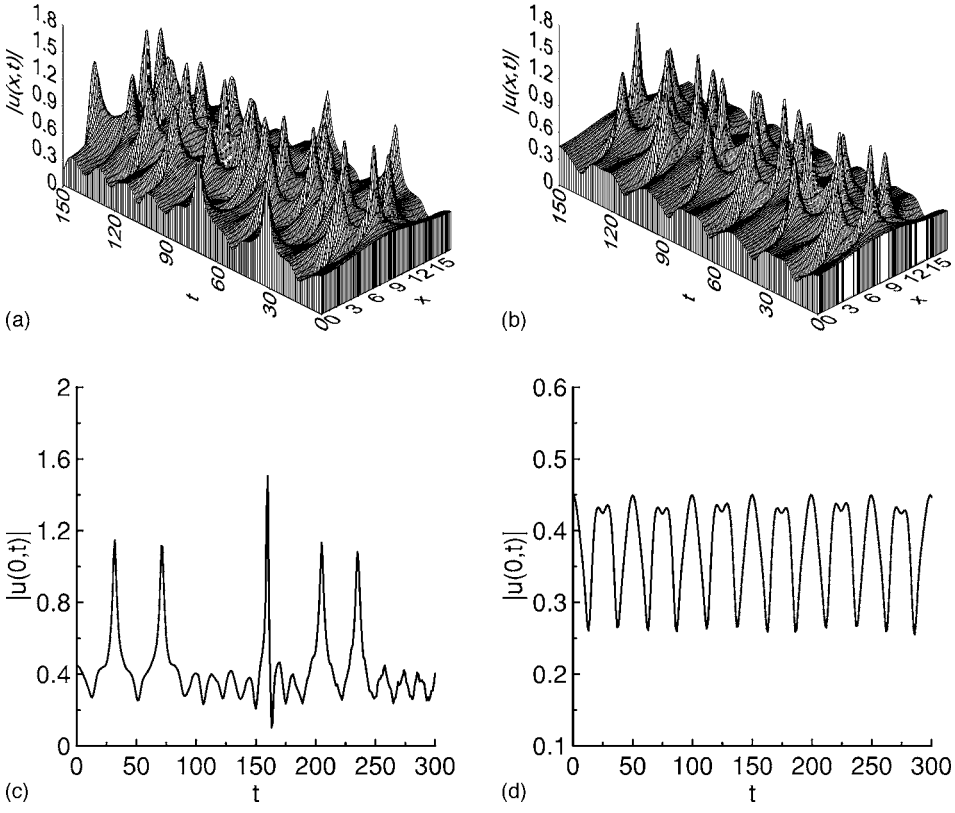

FIG. 4. Numerical simulations for the three-homoclinic-structure ($m=2$) problem: (a) and (b) are time-space evolution of the modulus of $u(x,t)$ over the first 150 time units; (c) and (d) are the time evolution of the modulus of $u(0,t)$ over the whole integration interval. The spatial resolution is $N_g=100$. Results in (a) and (c) are calculated from scheme CN, and those in (b) an (d) from schemes LB-III with IC-I.

As a concluding remark, the construction of the LB schemes for solving the one-dimensional cubic NLS equation can be easily extended to develop the LB schemes for the NLS equation in arbitrary number of dimensions and in the presence of other types of external potential. The initial condition for LBE considered in this paper can also be applied to other diffusion LB schemes in which passive scalar is the only essential conservation variable.

ACKNOWLEDGMENTS

The work was supported by the One Hundred Talents Project of the Chinese Academy of Sciences (Grant No. KCL 14014), the Engineering and Physical Sciences Research Council of United Kingdom (Grant No. GR/R72532).

[1] R. Benzi, S. Succi, and M. Vergassola, Phys. Rep. **222**, 145 (1992).
[2] S. Chen and G. D. Doolen, Annu. Rev. Fluid Mech. **30**, 329 (1998).
[3] D. A. Wolf-Gladrow, *Lattice-Gas Cellular Automata and Lattice Boltzmann Models: An Introduction* (Springer-Verlag, Berlin, Heidelberg, 2000).
[4] S. Succi, *The Lattice Boltzmann Equation: For Fluid Dynamics and Beyond* (Clarendon, Oxford, 2001).
[5] R. T. Bullough, P. M. Jack, P. W. Kitchenside, and R. Saunders, Phys. Scr. **20**, 364 (1979).
[6] K. Konno and H. Suzuki, Phys. Scr. **20**, 382 (1979).
[7] V. Zharnitsky, E. Grenier, K. R. T. J. Christopher, and S. K. Turitsyn, Physica D **152**, 794 (2001).
[8] S. C. Tsang, K. Nakkeeran, B. A. Malomed, and K. W. Chow, Opt. Commun. **249**, 117 (2005).
[9] D. H. Luo, J. Atmos. Sci. **62**, 5 (2005).
[10] D. H. Luo, J. Atmos. Sci. **62**, 22 (2005).
[11] M. J. Ablowitz and P. A. Clarkson, *Solitons, Nonlinear Evolution Equations and Inverse Scattering* (Cambridge University Press, Cambridge, 1991).
[12] M. Delfour, M. Fortin, and G. Payre, J. Comput. Phys. **44**, 277 (1981).
[13] D. Pathria and J. L. Morris, J. Comput. Phys. **87**, 108 (1990).
[14] Q. S. Chang, E. H. Jia, and W. Sun, J. Comput. Phys. **148**, 397 (1999).
[15] I. Bialynicki-Birula, Phys. Rev. D **49**, 6920 (1994).
[16] D. A. Meyer, J. Stat. Phys. **85**, 551 (1996).
[17] D. A. Meyer, Phys. Rev. E **55**, 5261 (1997).
[18] B. M. Boghosian and W. Taylor IV, Int. J. Mod. Phys. C **8**, 705 (1997).
[19] B. M. Boghosian and W. Taylor IV, Physica D **120**, 30 (1998).
[20] B. M. Boghosian and Washington Taylor IV, Phys. Rev. E **57**, 54 (1998).
[21] S. Succi and R. Benzi, Physica D **69**, 327 (1993).
[22] S. Succi, Phys. Rev. E **53**, 1969 (1996).
[23] S. Succi, Int. J. Mod. Phys. C **9**, 1577 (1998).
[24] J. Yepez, Int. J. Mod. Phys. C **9**, 1587 (1998).
[25] J. Yepez, Int. J. Mod. Phys. C **12**, 1273 (2001).
[26] J. Yepez, Int. J. Mod. Phys. C **12**, 1285 (2001).
[27] J. Yepez, J. Stat. Phys. **107**, 203 (2002).
[28] J. Yepez, Phys. Rev. E **63**, 046702 (2001).
[29] J. Yepez and B. Boghosian, Comput. Phys. Commun. **146**, 280 (2002).
[30] G. Vahala, J. Yepez, and L. Vahala, Phys. Lett. A **310**, 187 (2003).
[31] S. Chen, P. Dawson, G. D. Doolen, D. R. Janecky, and A. Lawniczak, Comput. Chem. Eng. **19**, 617 (1995).
[32] T. Inamuro, M. Yoshino, and F. Ogino, Phys. Fluids **9**, 3535 (1997).
[33] M. Junk, A. Klar, and L.-S. Luo, J. Comput. Phys. **210**, 676 (2005).
[34] R. R. Nourgaliev, T. N. Dinh, T. G. Theofanous, and D. Joseph, Int. J. Multiphase Flow **29**, 117 (2003).
[35] P. J. Dellar, Phys. Rev. E **64**, 031203 (2001).
[36] T. Toffoli and N. Margolus, Physica D **45**, 229 (1990).
[37] M. J. Ablowitz and B. M. Herbst, SIAM J. Appl. Math. **50**, 339 (1990).
[38] A. Caiazzo, J. Stat. Phys. **121**, 37 (2005).
[39] R. W. Mei, L.-S. Luo, P. Lallemand, and D. Humières, Comput. Fluids **35**, 855 (2006).